Geochemistry, Geophysics, Geosystems®

RESEARCH ARTICLE
10.1029/2022GC010673

Modeling Viscosity of Volcanic Melts With Artificial Neural Networks

D. Langhammer[1], D. Di Genova[1], and G. Steinle-Neumann[1]

[1]Bayerisches Geoinstitut, Universität Bayreuth, Bayreuth, Germany

Key Points:

- We train an artificial neural network that calculates temperature- and composition-dependent viscosity of volcanic melts
- The neural network reproduces and predicts experimental viscosity significantly better than previous global models
- A synthetic data approach based on the neural network is combined with a physical model to predict viscosity at eruptive temperatures

Supporting Information:

Supporting Information may be found in the online version of this article.

Correspondence to:

D. Langhammer,
dominic.langhammer@uni-bayreuth.de

Citation:

Langhammer, D., Di Genova, D., & Steinle-Neumann, G. (2022). Modeling viscosity of volcanic melts with artificial neural networks. *Geochemistry, Geophysics, Geosystems*, *23*, e2022GC010673. https://doi.org/10.1029/2022GC010673

Received 31 AUG 2022
Accepted 29 OCT 2022

Author Contributions:

Conceptualization: D. Langhammer, D. Di Genova, G. Steinle-Neumann
Data curation: D. Langhammer, D. Di Genova, G. Steinle-Neumann
Formal analysis: D. Langhammer, D. Di Genova, G. Steinle-Neumann
Funding acquisition: G. Steinle-Neumann
Investigation: D. Langhammer, D. Di Genova, G. Steinle-Neumann
Methodology: D. Langhammer, D. Di Genova, G. Steinle-Neumann
Project Administration: D. Di Genova, G. Steinle-Neumann

Abstract Viscosity is of great importance in governing the dynamics of volcanoes, including their eruptive style. The viscosity of a volcanic melt is dominated by temperature and chemical composition, both oxides and water content. The changes in melt structure resulting from the interactions between the various chemical components are complex, and the construction of a physical viscosity model that depends on composition has not yet been achieved. We therefore train an artificial neural network (ANN) on a large database of measured compositions, including water, and viscosities that spans virtually the entire chemical space of terrestrial magmas, as well as some technical and extra-terrestrial silicate melts. The ANN uses composition, temperature, a structural parameter reflecting melt polymerization and the alkaline ratio as input parameters. It successfully reproduces and predicts measurements in the database with significantly higher accuracy than previous global models for volcanic melt viscosities. Viscosity measurements are restricted to low and high viscosity ranges, which exclude typical eruptive temperatures. Without training data at such conditions, the ANN cannot reliably predict viscosities for this important temperature range. To overcome this limitation, we use the ANN to create synthetic viscosity data in the high and low viscosity range and fit these points using a physically motivated, temperature-dependent viscosity model. Our study introduces a synthetic data approach for the creation of a physically motivated model predicting volcanic melt viscosities based on ANNs.

Plain Language Summary Magma viscosity is a key parameter that controls the style of a volcanic eruption, whether it will be effusive or explosive. For this reason, any volcanic hazard mitigation plan requires detailed knowledge of this property. Melt viscosity can vary by up to 15 orders of magnitude (a factor of a quadrillion) with temperature and composition. Unfortunately, it is not possible to perform measurements over this range continuously in the laboratory, but only in two distinct temperature regimes, termed high and low viscosity ranges. In order to obtain a model to predict how composition and temperature control viscosity, we use machine learning and train an artificial neural network on a large viscosity database. This allows us to calculate high- and low-temperature viscosity data that we call synthetic. Since most magmas are erupted at temperatures between the high- and low-temperature ranges, we combine the synthetic data and a physically motivated equation to describe the dependence of viscosity on temperature. This model can compute viscosities in the region without measurements, including typical eruption temperatures of volcanoes. Our model serves the scientific community studying volcanic eruption mechanisms and its future prediction on a data driven basis.

1. Introduction

The shear viscosity (η) of volcanic melts is of great importance for the transport dynamics of magmas and the eruptive styles of volcanoes (Cassidy et al., 2018; Colucci & Papale, 2021; Di Genova et al., 2017; Dingwell, 1996; Gonnermann & Manga, 2007; Papale, 1999), making η an important quantity for physical volcanology. Melt viscosity depends dominantly on chemical composition (x) and temperature (T). Previous work has often used a T-dependent expression to fit data from η measurements to a specific anhydrous composition. Common examples are the Vogel-Fulcher-Tamman (VFT) (Fulcher, 1925; Tammann & Hesse, 1926; Vogel, 1921) and MYEGA (Mauro et al., 2009) models. With a critical influence of water on eruption dynamics (Gonnermann & Manga, 2013) and its strong control on viscosity, the dependence of η on H_2O is often considered separately in models. Such models are typically built by empirical modifications of the fitting parameters to include H_2O dependence (e.g., Dingwell et al., 1998; Giordano et al., 2009; Langhammer et al., 2021; Misiti et al., 2011; Robert et al., 2015; Vetere et al., 2006; Whittington, Hellwig, et al., 2009).

Software: D. Langhammer, D. Di Genova, G. Steinle-Neumann
Supervision: D. Di Genova, G. Steinle-Neumann
Validation: D. Langhammer, D. Di Genova
Visualization: D. Langhammer, D. Di Genova, G. Steinle-Neumann
Writing – original draft: D. Langhammer, D. Di Genova, G. Steinle-Neumann
Writing – review & editing: D. Langhammer, D. Di Genova, G. Steinle-Neumann

In contrast to the individual melt fits, global models predict viscosity based on x, T (Giordano et al., 2008; Hui & Zhang, 2007), and pressure P (Duan, 2014). These three global models are based on empirical descriptions and are fitted on large data sets. The complex and non-linear relation between chemical components, melt structure and viscosity prevents the use of a model approach based on physical principles. But advances in machine learning algorithms, specifically artificial neural networks (ANNs), provide an alternative route to describe the composition–viscosity relation. Using a large database, ANNs can find highly non-linear mappings between input and output without prior knowledge of the mathematical form of this connection (Aggarwal, 2018). Recently, Tandia et al. (2019) have shown the capabilities of ANN to accurately fit and predict melt η for a database of technical glasses. Based on this success, Cassar (2021) and Le Losq et al. (2021) produced ANN architectures using gray box approaches, trained on mostly technical glasses and the K_2O-Na_2O-Al_2O_3-SiO_2 (KNAS) system, respectively. In contrast to a black box approach, which directly maps the input parameters to the desired quantity (here η), their gray box approaches predict input parameters of certain viscosity equations (e.g., VFT or MYEGA) which are then used to compute η. This approach permits a physical interpretation of the predictions, within the constraints of the model.

However, with a scarcity of η data, this approach cannot be used for volcanic melts. The problem of sparse data is even more pronounced when considering the effect of water on η (Duan, 2014; Giordano et al., 2008; Hui & Zhang, 2007), ignored by all previous ANN-based models (Cassar, 2021; Le Losq et al., 2021; Tandia et al., 2019). Therefore, we do not follow the previous ANN studies with a gray box approach, but use a black box to utilize as many data as possible; this approach maps the input (composition x and T, where we treat H_2O on equal footing with the oxide components) directly to viscosity. We train an ANN using a database of viscosities for volcanologically relevant melts which we collected from the literature. We use 3,482 data points from 153 data sets (not counting variable H_2O content) for melts covering virtually the entire compositional space of magmas on Earth and some analogs of extraterrestrial melts (Figure 1). We show that our ANN is not only capable of fitting given data, but also of predicting η with high accuracy for the viscosity ranges in which measurements are performed.

To generate models that inter- and extrapolate in a physically sound way, which cannot be guaranteed using the black box approach, we combine the ANN with a "synthetic data" approach: For a composition of interest, we generate sets of η–T values from an ANN in two distinct η intervals in which viscosity measurements can be performed either by concentric cylinder (i.e., low viscosity, Lη, range: 10^{-3} Pa s $< \eta <$ 10^{5} Pa s) or micropenetration/parallel plate viscometry (i.e., high viscosity, Hη, range: 10^{8} Pa s $< \eta <$ 10^{13} Pa s). These isochemical η values are then fit using the MYEGA equation (Mauro et al., 2009) for T dependence. Our approach combines the accuracy of the neural network trained on a large data set of η values and the physical basis of the MYEGA equation. An application/calculator of our model is available at https://share.streamlit.io/domlang/visc_calc/main/final_script.py, the code and model can be found at https://github.com/DomLang/Visc_Calc.

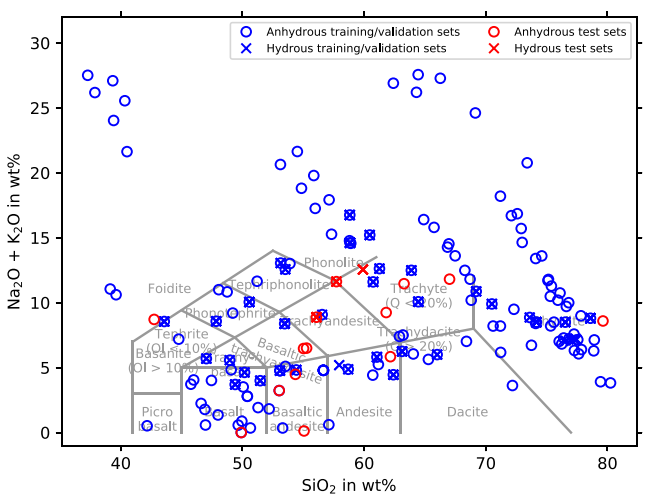

Figure 1. Total alkaline and silica content (Le Bas et al., 1986) for all data set in the database. Blue symbols indicate training/validation data sets and red symbols the test sets. Anhydrous data sets are shown by circles and hydrous ones by crosses. Values and references for the training/validation sets are given in Table 1 and for the test sets in Table 2.

2. Artificial Neural Networks

ANNs broadly refer to algorithms for pattern recognition, and here we make use of a simple architecture called a dense feed-forward multilayer perceptron (Aggarwal, 2018). It consists of three layer types: input, hidden and output (Figure 2). The layers contain so-called neurons, each storing a single numerical value. Each neuron of a layer is connected to every neuron in the following layer, hence dense, and every connection has a weight associated with it. The neuron values are propagated along these connections, and weights are optimized during the learning process, analogous to variable parameters when fitting an equation to data. The neurons of the input layer store the input data (Section 3.1) which are propagated through all neurons of the hidden layers until the output (η) is calculated. The output is compared to the corresponding measurement using a loss function (Abadi et al., 2015), for which we use the mean squared error. The loss function is minimized, going backwards through the network, tuning the weights. Furthermore,

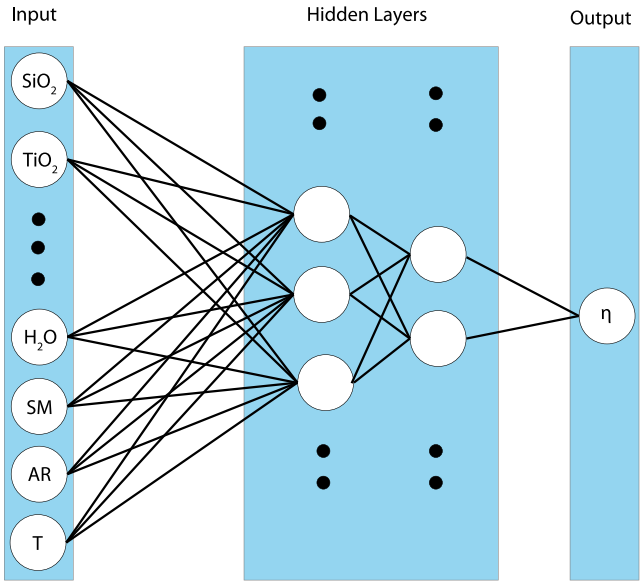

Figure 2. Sketch of a feed-forward multilayer perceptron. Circles are neurons storing single values. Each line connecting the neurons has a weight (regression parameter) and activation function associated with it. The black dots indicate that the number of neurons can be arbitrary. The number of hidden layers can vary; here, we illustrate two layers used for our artificial neural network.

non-linearity is added using so-called activation functions (Aggarwal, 2018) which can be applied to the values of each neuron before they are propagated further through the network. This way the hidden layers become a non-linear mapping between input and output.

3. Database

We compile a database of 3,482 tuples (T, x, η) for relevant melts from the literature. Of these, 2,538 are data from measurements of only anhydrous samples, while 193 data sets with the remaining 942 data contain H_2O. The data span a large chemical domain in the total alkaline-silica diagram (Figure 1). The database is separated into a training/validation (Table 1) and a test set (Table 2) with 3,194 and 288 data points, respectively. The training/validation set contains 144 rock types which yield a total of 320 compositions, counting each H_2O content as a unique composition. Of these, 142 are anhydrous and 178 hydrous. The test set contains 15 rock types and again taking into account differing H_2O contents, 29 unique measured compositions. Of these, 14 are anhydrous and 15 hydrous data sets. The test sets are chosen such that they probe a reasonable chemical domain to check the reliability of the predictions made by the ANN.

Silica content and the empirical parameter termed structure modifier content (SM, in mol%) (Giordano & Dingwell, 2003a) for one choice of the training and validation sets (Section 3.2) and for the test set are shown in Figure 3. The distributions for training and validation sets are very similar which indicates that the validation set tests the interpolation, not extrapolation, capabilities of a trained ANN. The SiO_2 content of data ranges from ∼37 wt% (∼40 mol%) to ∼80 wt% (∼85 mol%) and the H_2O content from 0 wt% to ∼6 wt% (∼16 mol%). Measured η for the Lη range from $\sim10^{-1}$ to $\sim10^{5}$ Pa s and for the Hη range from $\sim10^{8}$ to $\sim10^{14}$ Pa s. Temperature spans approximately 1180–2020 K and 590–1270 K in the Lη and Hη ranges, respectively (Figure 4).

3.1. General Data Preparation

In the training/validation set (Table 1) we initially consider anhydrous and hydrous data sets separately. They are each shuffled and then split into a training and validation set, according to ratios and procedures given in more detail in Section 3.2. The anhydrous and hydrous sets are then combined to finally yield training and validation sets containing both anhydrous and hydrous compositions. Since the number of hydrous data points is relatively small, this procedure ensures that there are sufficient hydrous data in the training set.

The input parameters and corresponding viscosity measurements of the training set are used for the regression during the learning process. After each learning cycle, the validation set is used to predict log η. As these data have not been used to train the neural network, the validation set evaluates the ANN's ability to generalize, that is, predict η. The loss function calculated from the validation set (validation loss) is also used to avoid overfitting. Overfitting is typically characterized as an increasing or constant validation loss, while the training loss keeps decreasing. This indicates that the ANN's ability to predict unknown values from input data remains constant or worsens despite an improving fit. The improvement in the fit is explained by the ANN learning the data by heart. To prevent overfitting and improve the ANN's ability to generalize, regularization methods such as dropout (Srivastava et al., 2014) can be used (Section 3.2).

As input parameters, we use mole fractions of SiO_2, TiO_2, Al_2O_3, FeO, Fe_2O_3, MnO, MgO, CaO, Na_2O, K_2O, P_2O_5, H_2O, temperature T in K, the SM parameter (Giordano & Dingwell, 2003a), and the alkali ratio $K_2O/(K_2O + Na_2O)$. Contrary to the global viscosity models by Hui and Zhang (2007) and Giordano et al. (2008) that consider the iron content in the melt as FeO only, we differentiate between FeO and Fe_2O_3. This distinction is important as Fe_2O_3 acts as a network former, leading to an increase in melt viscosity, while FeO acts as a network modifier and has the opposite effect on viscosity (Bouhifd et al., 2004; Chevrel et al., 2013; Dingwell &

Table 1
Data Sets Used in the Training and Validation Process, Listed With Decreasing SiO_2 Content

References	SiO_2	TA	H_2O	Name in source	References	SiO_2	TA	H_2O	Name in source
Hofmeister et al. (2014)	80.25	3.82		Moldavite	Giordano et al. (2006)	60.71	4.42		MST
Giordano et al. (2006)	79.43	3.91		MDV	Giordano et al. (2000)	60.46	15.21	0.00–3.75	
Le Losq and Neuville (2013)	78.92	7.13		NAK83.8.0	Giordano et al. (2009)	58.90	14.57		Mercato 1500
Di Genova et al. (2017)	78.87	6.29		F	Giordano et al. (2009)	58.84	14.61	0.00–4.24	Mercato 1600
Hess et al. (1995) and Dingwell et al. (1996)	78.60	8.80	0.00–3.35	HPG8	Whittington et al. (2001)	58.82	16.75	0.00–4.27	Phonolite
Di Genova et al. (2017)	77.86	6.39		G	Giordano et al. (2009)	58.80	14.77		Mercato 1400
Le Losq and Neuville (2013)	77.82	8.99		NAK83.8.2	Liebske et al. (2003)	58.69	4.87	0.00–1.96	Andesite
Di Genova et al. (2017)	77.63	6.06		A	Vetere et al. (2006)	57.95	5.19	2.73	MD25
Di Genova et al. (2017)	77.56	7.15		C	Vetere et al. (2006)	57.95	5.19	5.60	MD12
Di Genova et al. (2017)	77.28	6.32		B	Robert et al. (2019)	57.32	15.27		Jd100
Di Genova et al. (2017)	77.25	7.58		H	Robert et al. (2019)	57.12	17.92		Jd625
Di Genova et al. (2017)	76.83	7.22		D	Sehlke and Whittington (2015)	57.1	0.60		NVP
Le Losq and Neuville (2013)	76.81	10.00		NAK83.8.4	Liebske et al. (2003)	56.65	4.79		Unzen-A
Stabile et al. (2016)	76.62	9.71		Ebu-N-red	Liebske et al. (2003)	56.65	4.79		Unzen-3
Romine and Whittington (2015)	76.53	8.50	0.00–0.34	NCA	Liebske et al. (2003)	56.65	4.79		Unzen-2
Stabile et al. (2016)	76.40	7.28		Ebu-N	Liebske et al. (2003)	56.65	4.79		Unzen-4
Di Genova et al. (2017)	76.24	6.82		I	Liebske et al. (2003)	56.65	4.79		Unzen-5
Le Losq and Neuville (2013)	76.10	10.75		NAK83.8.6	Langhammer et al. (2021)	56.55	9.08	0.00–1.59	Lat-DSC
Goto et al. (2005)	76.03	7.02	0.00–0.58		Robert et al. (2019)	55.98	17.26		Jd75
Stabile et al. (2016)	75.92	10.19		Ebu-B-red	Robert et al. (2019)	55.86	19.79		Jd375
Hess et al. (1995)	75.60	8.50		5Mg	Robert et al. (2019)	54.85	18.81		Jd50
Stabile et al. (2016)	75.39	11.28		Ebu-C	Robert et al. (2019)	54.51	21.64		Jd0
Di Genova et al. (2017)	75.33	8.21		E	Robert et al. (2013)	54.42	4.82	0.00–3.76	sba
Stabile et al. (2016)	75.30	10.49		Ebu-B	Giordano et al. (2009)	53.90	13.01		Pompei TR
Stabile et al. (2016)	75.15	11.79		Ebu-C-red	Giordano et al. (2006)	53.53	5.09		MRP
Le Losq and Neuville (2013)	75.11	11.70		NAK83.8.8	Romano et al. (2003)	53.52	12.57	0.00–3.32	V_1631_W
Hess et al. (1995)	74.60	13.60		5K	Vetere et al. (2007)	53.47	8.38	0.00–4.75	Vul
Friedman et al. (1963)	74.16	8.50	0.00–1.25		Sehlke and Whittington (2015)	53.3	0.35		IcP-HCT
Hess et al. (1995)	74.10	13.40		5Na	Romano et al. (2003)	53.14	13.05	3.07	V_1631_G
Hess et al. (1995)	74.10	8.40		5Ca	Robert et al. (2019)	53.12	20.64		Jd25
Di Genova et al. (2017)	73.75	6.72		J	Robert (2014)	53.08	4.76	0.00–2.92	fu18
Whittington et al. (2004)	73.61	8.86	0.00–3.41	DK89	Hofmeister et al. (2016)	53.08	4.76		Bas-and
Stabile et al. (2016)	73.40	20.77		NFS-red	Sehlke and Whittington (2016)	53.02	3.23		CHW
Hofmeister et al. (2014)	72.99	14.64		Vase	Sehlke and Whittington (2016)	52.19	1.82		KREEPe
Hofmeister et al. (2014)	72.91	15.71		1960	Robert et al. (2015)	51.46	3.99	0.00–3.02	sb
Hofmeister et al. (2014)	72.59	16.85		1895	Sehlke and Whittington (2016)	51.28	1.92		SHG
Whittington, Bouhifd, and Richet (2009)	72.31	9.49		HP96	Giordano and Dingwell (2003a)	51.20	11.65		Ves_W_tot
Hofmeister et al. (2014)	72.19	3.62		Indoch	Sehlke and Whittington (2016)	50.65	0.35		KREEP
Hess et al. (1995)	72.10	16.70		10Na	Whittington et al. (2000)	50.56	10.05	0.00–2.27	Tephrite
Di Genova et al. (2017)	71.22	6.17		L	Hofmeister et al. (2016)	50.40	2.79		P-MPRB
Hess et al. (1995)	71.20	18.20		10K	Hofmeister et al. (2016)	50.40	2.79		MORB

Table 1
Continued

References	SiO_2	TA	H_2O	Name in source	References	SiO_2	TA	H_2O	Name in source
Hess et al. (1995)	71.20	8.20		10Mg	Misiti et al. (2009); Giordano et al. (2006)	50.17	4.63	0.00–4.16	SPZ, STB
Hess et al. (1995)	70.60	8.20		10Ca	Sehlke and Whittington (2016)	50.06	3.51		Mu-Fe
Langhammer et al. (2021)	70.50	9.90	0.00–3.55	Rhy14-DSC	Sehlke and Whittington (2016)	49.95	0.87		Lme
Di Genova et al. (2013)	69.21	10.87	0.00–3.55	PS-GM	Al-Mukadam et al. (2020)	49.90	0.00		Di
Stabile et al. (2016)	69.14	24.61		NFS	Sehlke and Whittington (2016)	49.65	0.57		KOM
Giordano et al. (2006)	68.80	10.19		CL_OF	Robert et al. (2015)	49.40	3.70	0.00–2.7	fu06
Le Losq and Neuville (2013)	68.71	11.81		NAK75.12.0	Giordano and Dingwell (2003a)	49.20	9.20		Ves_G_tot
Hofmeister et al. (2016)	68.41	7.02		Rhyo-dac	Giordano et al. (2006)	49.07	4.83		STR
Le Losq and Neuville (2013)	68.28	12.49		NAK75.12.2	Langhammer et al. (2021)	48.95	5.57	0.00–2.4	Bas1-DSC
Le Losq and Neuville (2013)	67.48	13.61		NAK75.12.5	Giordano et al. (2009)	48.74	10.83		Pollena GM
Le Losq and Neuville (2013)	66.96	14.53		NAK75.12.7	Giordano et al. (2009)	48.05	11.00		Pollena TR
Le Losq and Neuville (2013)	66.85	14.28		NAK75.12.6	Morrison et al. (2019)	47.99	1.35		NOR
Stabile et al. (2016)	66.26	27.28		KFS	Giordano et al. (2009)	47.84	8.57	0.00–4.45	1906GM
Giordano and Dingwell (2003a)	66.00	6.00	0.00–1.98	UNZ	Hofmeister et al. (2016)	47.45	4.01		OIB1
Le Losq and Neuville (2013)	65.75	15.80		NAK75.12.10	Giordano and Dingwell (2003b)	47.03	5.69	0.00–2.31	ETN
Alidibirov et al. (1997)	65.28	5.63			Sehlke and Whittington (2016)	46.96	0.58		EUC
Le Losq and Neuville (2013)	64.90	16.40		NAK75.12.12	Morrison et al. (2019)	46.91	1.78		ANOR
Whittington et al. (2001)	64.45	10.07	0.00–4.92	Trachyte	Sehlke and Whittington (2016)	46.60	2.24		NAK
Stabile et al. (2016)	64.44	27.56		KFS-red	Morrison et al. (2019)	45.99	4.05		JSC-1a
Hess et al. (1995)	64.30	26.20		20K	Giordano et al. (2006)	45.76	3.72		SLP
Hofmeister et al. (2016)	64.04	6.05		Dac-and	Morrison et al. (2020)	44.76	7.19		NYI-1948
Giordano et al. (2004)	63.88	12.49	0.00–3.86	MNV	Whittington et al. (2000)	43.57	8.55	0.00–2.06	NIQ
Hess et al. (1995)	63.20	7.50		20Mg	Sehlke and Whittington (2016)	42.16	0.52		LM
Whittington, Hellwig, et al. (2009)	63.12	6.25	0.00–5.04	BRD	Robert et al. (2019)	40.51	21.63		Ne100
Hess et al. (1995)	62.90	7.40		20Ca	Robert et al. (2019)	40.33	25.55		Ne625
Richet et al. (1996)	62.40	4.45	0.00–3.46	Andesite	Morrison et al. (2020)	39.61	10.61		NYI-1977
Hess et al. (1995)	62.40	26.90		20Na	Robert et al. (2019)	39.41	24.03		Ne75
Romano et al. (2003)	61.26	12.62	0.00–3.78	AMS_B1	Robert et al. (2019)	39.34	27.09		Ne375
Neuville et al. (1993)	61.17	5.24		Andesite	Sehlke and Whittington (2016)	39.13	11.05		NYI
Hellwig (2006)	61.05	5.81	0.00–4.94	Dacite	Robert et al. (2019)	37.87	26.18		Ne50
Giordano et al. (2004)	60.74	11.60	0.00–3.41	IGC	Robert et al. (2019)	37.28	27.51		Ne25

Note. Oxide compositions and H_2O are given in wt%. The H_2O content is given as the range found in the respective reference. TA = $Na_2O + K_2O$ states the total alkali content (wt%). The first column gives the reference from which the data are taken, the last column indicates the sample name used in the respective publication. Detailed oxide compositions of the melts listed here are given in Data Set S1.

Virgo, 1987; Kolzenburg et al., 2018; Liebske et al., 2003; Stabile et al., 2021; Vetere et al., 2008). For samples with only the total iron content FeO_{total} reported, we distribute it evenly between FeO and Fe_2O_3 with a factor of 1.11 to account for the higher molar weight of Fe_2O_3 (Langhammer et al., 2021). SM reflects the degree of structural polymerization on η, and the alkali ratio is known to significantly affect the viscosity of SiO_2-rich systems (Di Genova et al., 2017; Le Losq & Neuville, 2013; Stabile et al., 2016). Cr_2O_3 is only used during the conversion from wt% to mole fractions. It is omitted during the training as the vast majority of compositions contain <0.02 wt%.

Table 2
Data Sets Used for Testing the Artificial Neural Network, Listed With Decreasing SiO_2 Content

References	SiO_2	TA	H_2O	Name in source
Hofmeister et al. (2014)	79.63	8.59		Haplogranite
Webb (2021)	67.02	11.81		h16b
Webb (2021)	63.28	11.46		h22b
Hofmeister et al. (2016)	62.16	5.84		Dacite
Webb (2021)	61.81	9.24		h5a
Misiti et al. (2006)	59.90	12.55	0.18–5.81	AMS
Langhammer et al. (2021)	57.72	11.62	0.00–4.78	Tra3-DSC
Misiti et al. (2011)	56.08	8.88	0.00–3.28	FR
Webb (2021)	55.27	6.50		h34
Sehlke and Whittington (2015)	55.06	0.12		Enstatite Basalt
Sehlke and Whittington (2015)	55.02	6.47		NVP-Na
Webb (2021)	54.35	4.48		h10
Hofmeister et al. (2016)	53.02	3.23		Dolerite
Al-Mukadam et al. (2020)	49.90	0.00		Di, DSC derived viscosities
Webb (2021)	42.74	8.71		NIQ

Note. Oxide compositions and H_2O are given in wt%. H_2O is given as the range found in the respective reference. TA = $Na_2O + K_2O$ states the total alkali content (wt%). The first column gives the reference from which the data are taken, the last column indicates the sample name used in the respective publication. Detailed oxide compositions of the melts listed here are given in Data Set S2.

To improve convergence and stability of the training process we scale the input data as follows (Montavon et al., 2012): (a) mole fractions of composition lie in the interval [0, 1], (b) T is normalized by dividing all values by the largest T within the data set (2023 K for Ne375, Table 1). (c) We modify the definition of SM using mole fractions, also leading to values in the interval [0, 1]. (d) Finally, for every value of each input parameter x_i the z-score (Cassar, 2021) is calculated as input according to

$$z_{i,j} = \frac{x_{i,j} - \mu_i}{\sqrt{\sigma_i^2}}, \tag{1}$$

$$\mu_i = \frac{1}{N}\Sigma_{j=1}^{N} x_{i,j}, \tag{2}$$

$$\sigma_i^2 = \frac{1}{N}\Sigma_{j=1}^{N}(x_{i,j} - \mu_i)^2. \tag{3}$$

Here, $x_{i,j}$ and $z_{i,j}$ denote the jth value of the ith input parameter (e.g., SiO_2 content), x denoting the old, and z the z-score used as input for the ANN. μ_i is the average and σ_i^2 the variance of the input. The scaling achieves an average of 0 and variance of 1 for the new input z_i. Values for μ and σ^2 can be found in Table S1 in Supporting Information S1.

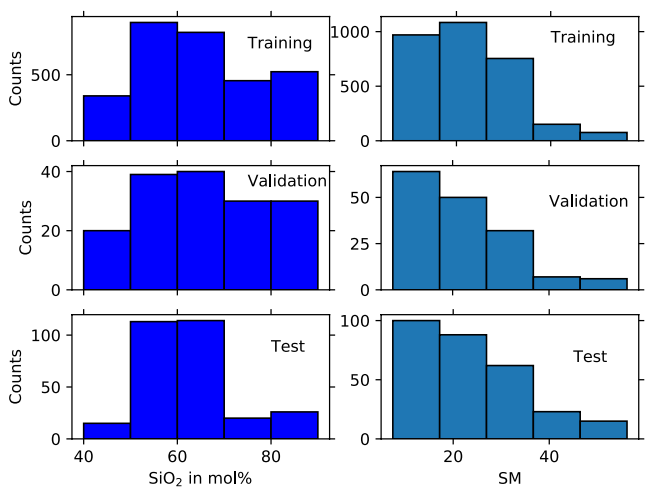

Figure 3. Histograms indicating the data distribution for one choice of the training, validation and test sets in terms of SiO_2 content (left column) and structure modifier structural parameter (right column).

3.2. Training Procedure

Critical parameters for training an ANN (hyperparameters) are the number of hidden layers and neurons per layer which, through the associated weights, define the number of adjustable parameters, the learning rate which defines the step size during training, and the dropout value. The dropout randomly sets outputs of a layer to zero at a probability given by the dropout value. This simulates various different ANNs during a training session and reduces

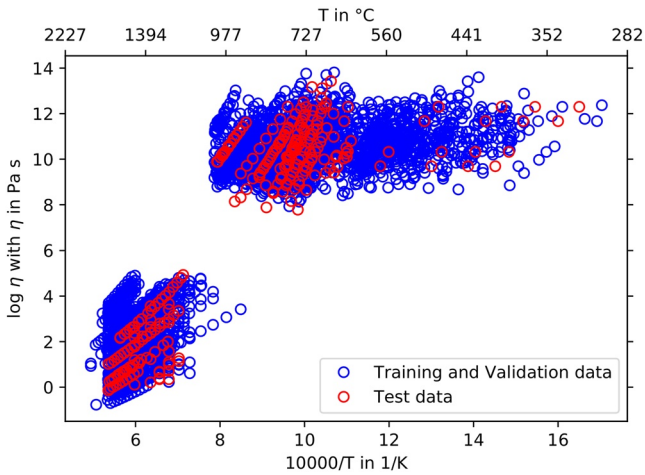

Figure 4. Viscosity (log η) values from the data sets used here as a function of inverse temperature (10,000/T). Data shown in blue are used in the training/validation process (Table 1), red circles mark the test set (Table 2).

overfitting (Srivastava et al., 2014). As a measure for the quality of the ANN we use the root-mean-square-error (RMSE), commonly used in other publications. To search the space of hyperparameters, we use Bayesian optimization as a stochastic algorithm (Aggarwal, 2018; Snoek et al., 2012) to find architectures with low validation errors. In this step, we perform the shuffling described above and combine 90% of the anhydrous and hydrous data sets each to the training set and the remaining 10% to the validation set.

In the Bayesian optimization, we fix several hyperparameters: (a) We use two hidden layers. Several tests have shown little improvement when using three layers, and increasing the number of layers further increases the complexity which is not desired in our case given the scarcity of data. (b) We apply the Adam optimizer (Kingma & Ba, 2014) as an algorithm, including the amsgrad flag (Reddi et al., 2019). (c) For activation in all hidden layers, we use the leaky ReLU function defined as

$$f(x) = \alpha x \quad \text{for } 0 > x, \tag{4}$$

$$f(x) = x \quad \text{for } 0 \leq x. \tag{5}$$

We use the default value of $\alpha = 0.3$ (Abadi et al., 2015). In the in- and output-layers identity is used as activation. (d) As batch size, we use the complete training set (full batch).

For other hyperparameters we vary the range (Table 3): (a) The number of neurons in the hidden layers explored is $1 - 256$ per layer, with final values of 256 for the first and 208 for the second layer. The value of 256 in the first layer corresponds to the upper bound; due to the small number of data available and only small improvements during test runs with an increased threshold, we choose to use 256, nevertheless. This avoids increasing the complexity and computational expense while retaining an accurate model, as shown in the following sections. (b) For the learning rate we use 0.057317962127906, after exploring $0.00001 - 0.5$. (c) From a range of $0.0 - 0.5$, the chosen dropout value is 0.16569639948335368.

Using the ANN hyperparameters chosen by the Bayesian optimization, we apply a 20-fold cross-validation process. All anhydrous and hydrous data sets in the training/validation database (Table 1) are shuffled separately and split into 20 sets each; one of each is combined to create 20 sets that contain anhydrous and hydrous data (superset). The ANN is trained 20 times, using 19 of the supersets for training and one as validation. The validation superset is exchanged until each superset was used for validation once. These architectures are used to predict all η values of the test set, and we present and discuss results for the ANN with the lowest RMSE.

Neural networks are built using TensorFlow (Abadi et al., 2015) and the Bayesian optimization is performed with the KerasTuner (O'Malley et al., 2019), using Python as programming language. Data is managed and prepared using the Pandas (Reback et al., 2021) and NumPy (Harris et al., 2020) packages.

4. Training Results and Evaluation

The SiO_2 distribution for the training and validation set belonging to the network that displays the lowest RMSE when predicting the test set is very similar (Figure 3). Their RMSE values are 0.09 and 0.12, respectively (Figure 5). Therefore we expect the ANN to be trained to interpolate rather than extrapolate. This in turn leads us to recommend the use of this model only within the, albeit extensive, chemical bounds given by the training/validation data set (Figure 1). The models of Hui and Zhang (2007) and Giordano et al. (2008) applied to the training/validation sets in our database produce RMSE values of 1.36 and 1.18, respectively (Figure S1 in Supporting Information S1).

For the test sets, we compare measured η to predictions of our ANN and the global models of Hui and Zhang (2007) and Giordano et al. (2008) in Figure 6. The ANN predictions show the lowest RMSE with 0.45, compared

Table 3
Range of Explored Hyperparameters and Final Results From the Baysian Optimization

Hyperparameter	Range	Result
Neurons in Layer 1	1–256	256
Neurons in Layer 2	1–256	208
Learning rate	0.00001–0.5	0.05731796
Dropout	0.0–0.5	0.1656964

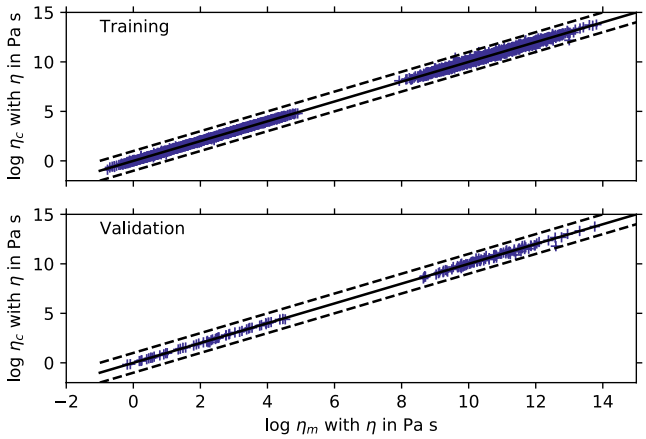

Figure 5. Calculated (log η_c) versus measured (log η_m) viscosities of the training (top) and validation sets (bottom) for the artificial neural network yielding the lowest root-mean-square-error (RMSE) when applied to the test sets. The black solid line indicates the one to one correspondence, and dashed lines ±1 log-unit deviation from identity. RMSE values are 0.09 for the training and 0.12 for the validation set.

to 0.89 and 1.23 for the models by Hui and Zhang (2007) and Giordano et al. (2008), respectively.

Both literature models show significantly larger deviations than the ANN prediction for specific data sets. The model by Hui and Zhang (2007) overestimates viscosity measurements for the enstatite and a Na_2O-rich basalt (NVP-Na) by Sehlke and Whittington (2015) and for the diopside (Di) determined from calorimetry experiments by Al-Mukadam et al. (2020). The model by Giordano et al. (2008) underestimates viscosities for these samples as well as for a haplogranite (Hofmeister et al., 2014). The two compositions by Sehlke and Whittington (2015)—models for basalts on Mercury—show a high content in CaO and MgO as does the Di by Al-Mukadam et al. (2020) (Data Set 2), outside typical terrestrial compositions. It may therefore not be surprising that the models by Hui and Zhang (2007) and Giordano et al. (2008) fail to reliably predict their η, while the training/validation set of our ANN contains two similar compositions from Sehlke and Whittington (2015) and further planetary tholeiitic melts (Sehlke & Whittington, 2016).

The high η for the fully polymerized haplogranite by Hofmeister et al. (2014) is not reproduced well by the model of Giordano et al. (2008) which also shows a poor fit for a similar model haplogranite (HPG8) by Hess et al. (1995).

5. Synthetic Models

Eruptive T of most magmas lie between the Hη and Lη range. At these T, volcanic melts tend to crystallize faster than the timescale of the η measurement. Therefore an interpolation—or extrapolation if data only exist at Hη—between these ranges is required to determine η. This is done by fitting η data using models such as the MYEGA and VFT equations (Figure 7), sometimes modified to include a H_2O dependence. Contrary to MYEGA fits to experimental data, viscosities directly determined from the ANN in the range 10^5 Pa s < η < 10^8 Pa s show strong deviations from expected behavior for some melt compositions (Figure 7). This is not surprising given the fact that the ANN is not trained in this η range due to the experimental gap discussed in the Introduction.

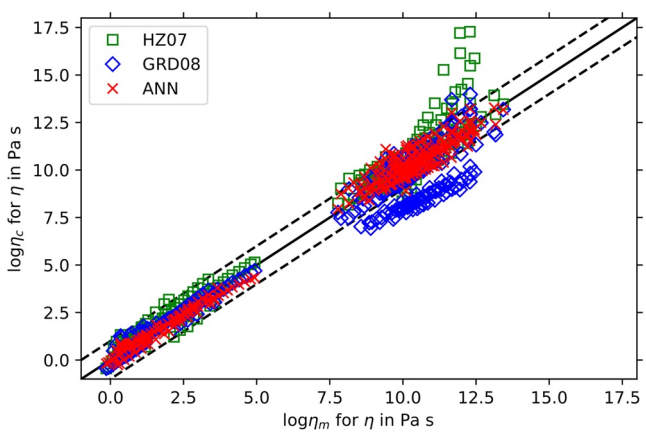

Figure 6. Comparison of calculated (log η_c) and measured (log η_m) viscosities for the artificial neural network (ANN, red crosses, RMSE = 0.45), the model by Giordano et al. (2008) (GRD08, blue diamonds, RMSE = 1.23) and Hui and Zhang (2007) (HZ07, green squares, RMSE = 0.89) for melts in the test sets. The one to one correspondence is shown by the solid black line, dashed lines indicate a ±1 log-unit deviation from identity.

5.1. Creating a Synthetic Model

Mimicking the fitting of experimental data, we create a set of synthetic data from the ANN in the Hη and Lη ranges and fit the physically motivated MYEGA equation (Mauro et al., 2009),

$$\log \eta = A + (12 - A)\frac{T_g}{T}\exp\left[\left(\frac{m}{12 - A} - 1\right)\left(\frac{T_g}{T} - 1\right)\right], \quad (6)$$

to them. The viscosity at infinite T, $A := \log \eta_\infty$, melt fragility m and glass transition temperature T_g (for log η = 12) are fitting parameters. We fix $A = -2.9$ (Zheng et al., 2011), following our previous work and discussion (Langhammer et al., 2021), creating a two-parameter model equation for a specific composition that can be used to calculate η over a wide T range.

Determining the Hη and Lη intervals for which synthetic data are created is an important step in the process, as this choice strongly influences the model parametrization. We examine the distributions of log η for the whole database (Figure 8) to choose appropriate intervals for the Hη and Lη ranges. In the Hη region, the data density is highest at log η between 10 and 11, and we create synthetic data in 1-log around the maximum, that is, in the interval [9.5, 11.5] with a step size of log η = 0.5. Data coverage in the Lη region varies with SiO_2 content, and we split the data sets at 60 wt% SiO_2. With broad maxima for log η between 0.5 and 1.5 ($SiO_2 \leq 60$ wt%)

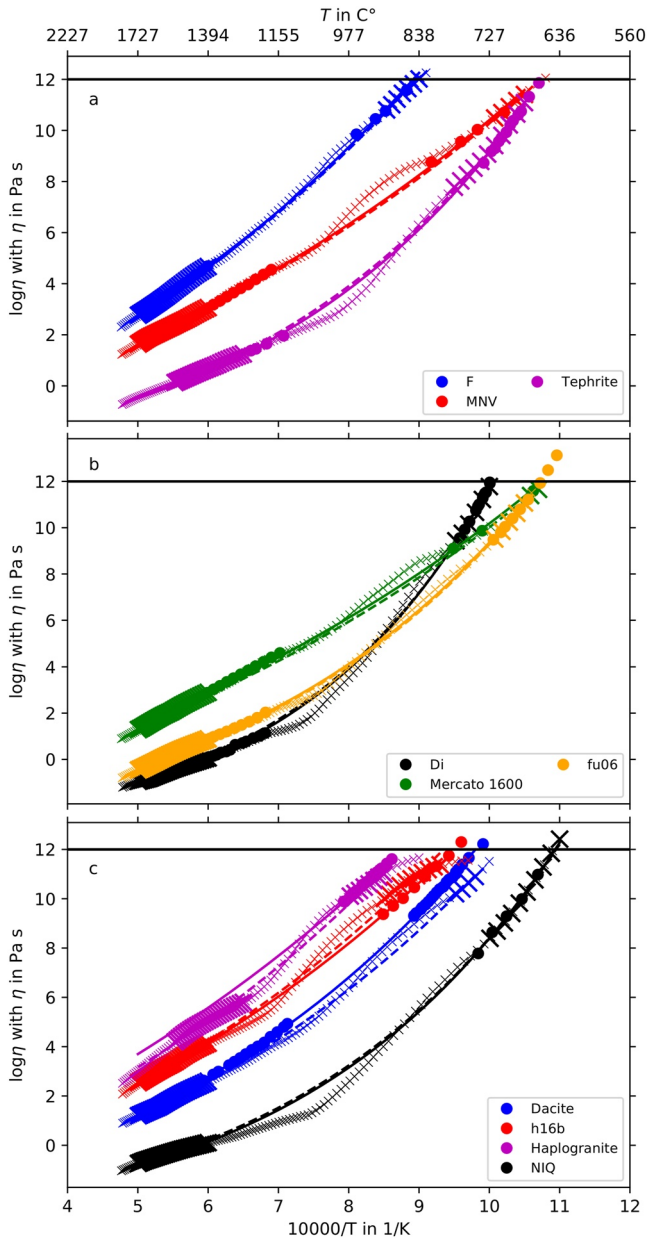

Figure 7. Viscosity (log η) as a function of inverse temperature (10,000/T) for some anhydrous compositions in the training/validation database (a and b) and the test set (c). Measurements are shown by filled circles, viscosity values predicted from the artificial neural network by crosses, where bold crosses indicate the η range for the synthetic data approach. Solid (dashed) lines show MYEGA fits to the experimental (synthetic) data. Data references can be found in Tables 1 and 2. The horizontal lines indicate 10^{12} Pa s.

and log η between 2.5 and 3.5 (SiO_2 > 60 wt%), we create synthetic data in the log η intervals [0, 2] and [2, 4.5], respectively, again in steps of log η = 0.5. Such a split is not necessary in the Hη range due to very similar distribution of data (Figure 8).

Technically, we use the ANN in conjunction with the bisection method to calculate T for the previously discussed log η values to a precision of 10^{-5}. The log $\eta - T$ dependence is fit using the MYEGA model (Equation 6 with $A = -2.9$). A web application which follows this scheme and calculates the MYEGA parameters and a viscosity value for a desired T can be found at https://share.streamlit.io/domlang/visc_calc/main/final_script.py. It is important to mention, that if the composition which is entered into the app only reports FeO_{total}, one must split it according to $FeO = FeO_{total}/2$ and $Fe_2O_3 = FeO_{total}\frac{1.11}{2}$. On the other hand, if the compositions reports the total iron as Fe_2O_{3total} it must be split according to $FeO = \frac{Fe_2O_{3total}}{(2{\cdot}1.11)}$ and $Fe_2O_3 = Fe_2O_{3total}/2$. Fitting parameters m and T_g can be used for further calculations. A Table S2 to calculate η values from the fit parameters m and T_g for various temperatures is supplied in Supporting Information.

5.2. Testing Synthetic Models

A comparison between the MYEGA fit to ANN viscosities (synthetic model) and experimental data for the compositions in the training/validation set (Figure 9a) already used in Figure 7 and discussed in Section 4 shows that the experimental measurements agree well with the ANN predictions where they overlap, both in the Lη and Hη ranges. The synthetic fit describes the experimental T dependence of η measurements reasonably well, except for Mercato 1600 (Giordano et al., 2009) that shows a more Arrhenian behavior in experiments. This discrepancy stems from the fact that, with a SiO_2 content of 58.84 wt%, the synthetic model is based on ANN viscosities in the log η interval [0, 2], while experiments cover log η in a range 2 − 4.6. However, the direct ANN predictions reproduce measured η for Mercato 1600 quite well (Figure 7b).

A similar behavior can be seen for samples from the test set in Figure 9b. The viscosity for three of the four compositions is described well, but values for the Dacite by Hofmeister et al. (2016) are predicted lower than the measurements by 0.9 − 0.7 log-units (decreasing with T) in the Hη range, while η of two Fe-free synthetic dacites in the training/validation set (Hellwig, 2006; Whittington, Hellwig, et al., 2009) are reproduced well. Evaluating the same compositions with the global model by Giordano et al. (2008) reveals that it has a similar problem predicting η for the Dacite by Hofmeister et al. (2016) although to a slightly smaller extent (0.7 − 0.5 log-units). As our model reproduces the experimentally measured η for the Dac-and by Hofmeister et al. (2016) with a similar iron content well, the reason for this specific discrepancy remains unclear.

The RMSE value for η in the training/validation set is 0.20 (Figure 10), slightly worse than those from the ANN directly (0.09 and 0.12 for training and validation, respectively). For the test set, the values are 0.45 for the ANN predictions and 0.52 for the synthetic model, respectively. In comparison to RMSE values of 1.36 and 1.18 for the entire database by the global models of Hui and Zhang (2007) and Giordano et al. (2008), respectively, the synthetic model provides quite accurate results, and has a physical basis with the MYEGA equation. For the 32 compositions in the KNAS system in our training/validation database (Table 1), our model performs better than the one by Le Losq et al. (2021), with values of RMSE = 0.29 and RMSE = 0.39, respectively (Figure S2

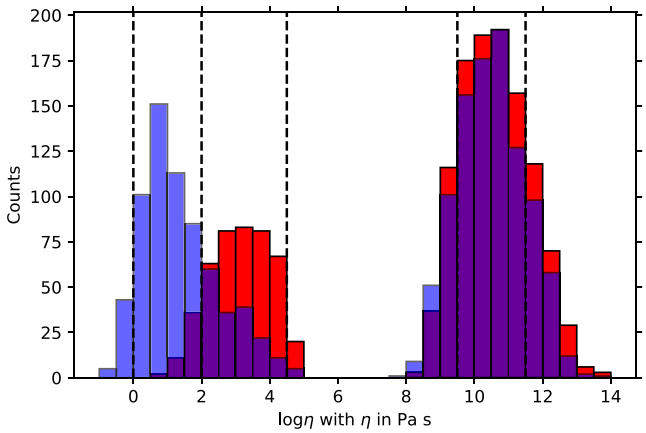

Figure 8. Distribution of viscosities in the training/validation database in the Hη and Lη regions, binned with log $\eta = 0.5$ intervals. Data sets in both regions are split into compositions with $SiO_2 < 60$ wt% (blue) and $SiO_2 \geq 60$ wt% (red). Purple indicates the overlap of distributions. The vertical dashed lines indicate the log η ranges over which we create synthetic data, that is, [9.5, 11.5] at Hη for all compositions, and at Lη [0, 2] or [2, 4.5] for melts containing $SiO_2 < 60$ wt% and $SiO_2 \geq 60$ wt%, respectively.

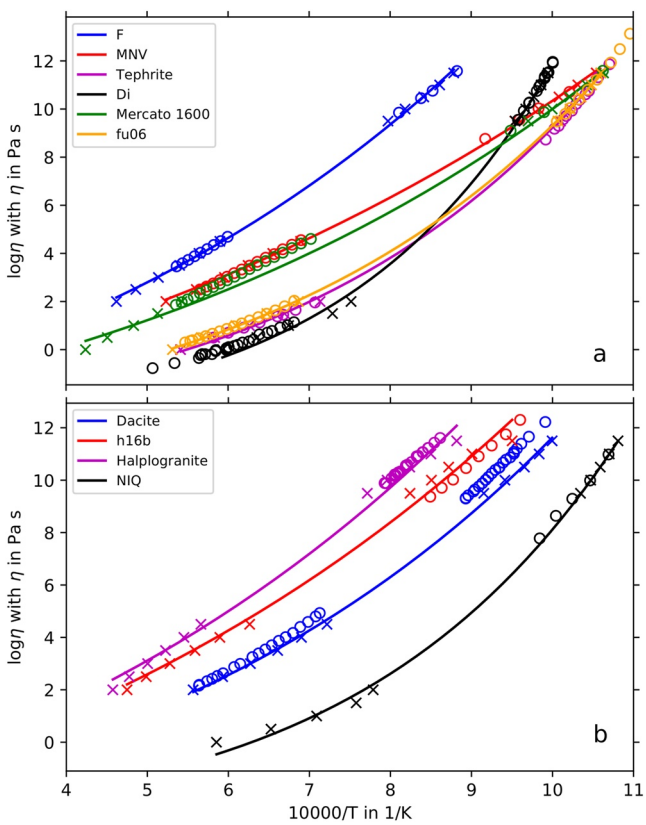

Figure 9. Comparison of fits to synthetic data (log η vs. $1/T$) to measurements for the compositions also used in Figure 7 (training/validation sets in panel (a), test sets in panel (b)). Crosses are the synthetic data and lines are MYEGA fits (Mauro et al., 2009) to them. Circles are the respective measurements. Data references can be found in Tables 1 and 2.

in Supporting Information S1). The model of Le Losq et al. (2021) can not be applied to natural volcanic melts in a meaningful way, as these typically contain divalent cations, most importantly MgO, CaO and FeO as well as water.

The parameters for the MYEGA model (Equation 6) do not differ significantly for T_g from the individual isochemical fits (Figure 11 and Figure S3 in Supporting Information S1) and the direct ANN inversion. For a reasonable comparison, only samples which include measurements in the Hη and Lη range from the training/validation set are included in Figure 11 and Figure S3 in Supporting Information S1. RMSE values of 18.3 and 7.16 K for the direct ANN inversion and the synthetic model, respectively, reflect the narrow distribution in Figure 11 and Figure S4 in Supporting Information S1, and an average difference of $\delta T_g = -0.5$ K between the direct MYEGA fit and the synthetic model (Figure S3 in Supporting Information S1) show that the synthetic model approach used here does not introduce any bias. Values of melt fragility m derived from synthetic data tend to be slightly overestimated (Figure S4 in Supporting Information S1), with the average deviation from direct MYEGA fits of $\delta m = 1.04$. A quasi-linear trend of increasing m with structural parameter SM discussed in Langhammer et al. (2021) is reproduced well.

The expected reduction in viscosity due to increased water content is also reproduced by our model. This includes both a reduction in T_g and m with increasing H_2O content (Figure S5 in Supporting Information S1).

6. Conclusion

In this work we have trained an ANN on a database containing 3,194 temperature-dependent viscosity (η) measurements for volcanic melts spanning a large chemical domain, including extraterrestrial model systems. The neural network takes melt composition, H_2O content, temperature T, the chemical parameters SM, reflecting melt polymerization, and the alkaline ratio $K_2O/(Na_2O + K_2O)$ as input to predict η. We show that the trained neural network describes the data in the database very well, significantly better than commonly used global models (Giordano et al., 2008; Hui & Zhang, 2007). In this context, it is worth emphasizing that—contrary to such models—the ANN relies on data only, and does not assume a functional dependence of viscosity. As such, interactions between different compositional components are taken into account implicitly. This suggests that despite the relatively scarce viscosity data for volcanic melts the success of ANN previously demonstrated for technical glasses (Cassar, 2021; Tandia et al., 2019) can be transferred to volcanology. To facilitate an easy use of our trained ANN, we make an online viscosity calculator available at https://share.streamlit.io/domlang/visc_calc/main/final_script.py.

The lack of training data in an η range $10^5 - 10^8$ Pa s for T characteristic for volcanic eruptions results in unphysical behavior of η. We therefore combine the reliable ANN predictions of η in the ranges where training data is available at high and low viscosity with a fit using the MYEGA equation to achieve a physically sound interpolation for geologically relevant conditions. The relevant parameters can be calculated using the web application mentioned in the previous paragraph. An Table S2 to calculate viscosities using these parameters and the MYEGA equation (Mauro et al., 2009) is supplied in Supporting Information S1.

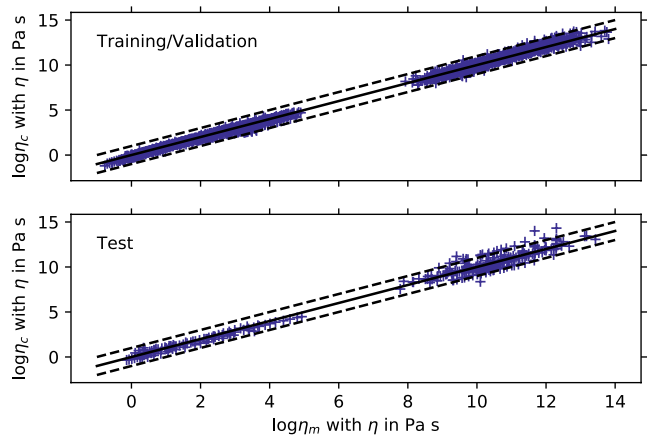

Figure 10. Comparison of viscosity values predicted by the synthetic models (log η_c) to measurements (log η_m) of the training/validation (top) and test (bottom) sets. The solid line shows the one to one correspondence, with the dashed lines ±1 log-unit deviations from identity. The respective root-mean-square-error values are 0.2 (top) and 0.52 (bottom).

Creating more accurate and versatile neural networks for melt viscosity, and other properties in general, is only limited by the quality and quantity of data. The time-consuming task of guessing a model equation and assuming critical parameters for melt characteristics is partly eliminated, while physical behavior of the melt is implicitly included in the modeling process. With more data and further analysis, these implicit physical relations may reveal themselves and lead to a better understanding on composition-structure-property relations. Our results hopefully encourage other researchers to further explore machine learning algorithms in the context of natural silicate melts and volcanology.

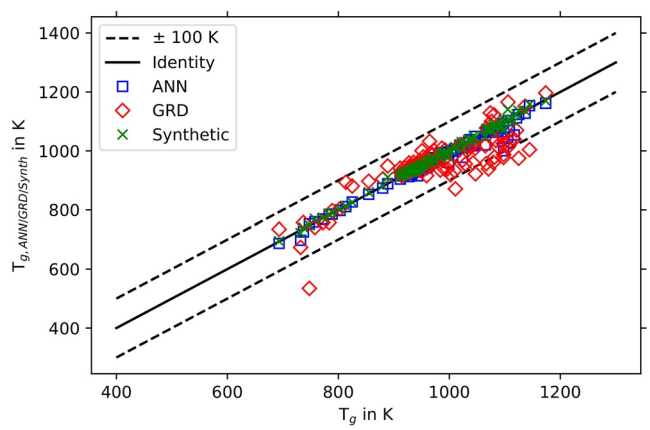

Figure 11. Comparison of calculated T_g values for compositions from the training/validation database. T_g on the x-axis are from isochemical MYEGA fits of the experimental data, on the y-axis T_g calculated from the artificial neural network (ANN) directly (squares), from the synthetic data approach (crosses) and from the model of Giordano et al. (2008) (GRD, diamonds) are shown. Only samples with measurements in both the Lη and Hη ranges in Table 1 are used. Root-mean-square-error values are 18.3 K for the ANN, 7.16 K for the fit to synthetic data, and 57.53 K for the GRD model.

Data Availability Statement

The training, validation and testing data, the trained ANN, and the code for the web application (https://share.streamlit.io/domlang/visc_calc/main/final_script.py) are available at https://github.com/DomLang/Visc_Calc (https://doi.org/10.5281/zenodo.7317803).

Acknowledgments
The authors acknowledges funding by the Deutsche Forschungsgemeinschaft (DFG) to DDG (Grant DI 2751/2-1) and GSN (STE1105/13-2 within the Research Unit FOR2440). References to all data used in this study are documented in Tables 1 and 2, and compositions of the melts are tabulated in Data Sets S1 and S2. An Table S2 to calculate viscosities from the MYEGA equation is included in Supporting Information S1. Open Access funding enabled and organized by Projekt DEAL.

References

Abadi, M., Agarwal, A., Barham, P., Brevdo, E., Chen, Z., Citro, C., et al. (2015). TensorFlow: Large-scale machine learning on heterogeneous systems [Software]. Retrieved from https://www.tensorflow.org/

Aggarwal, C. C. (2018). *Neural networks and deep learning*. Springer.

Alidibirov, M., Dingwell, D. B., Stevenson, R. J., Hess, K.-U., Webb, S. L., & Zinke, J. (1997). Physical properties of the 1980 Mount St. Helens cryptodome magma. *Bulletin of Volcanology*, *59*(2), 103–111. https://doi.org/10.1007/s004450050178

Al-Mukadam, R., Di Genova, D., Bornhöft, H., & Deubener, J. (2020). High rate calorimetry derived viscosity of oxide melts prone to crystallization. *Journal of Non-Crystalline Solids*, *536*, 119992. https://doi.org/10.1016/j.jnoncrysol.2020.119992

Bouhifd, M. A., Richet, P., Besson, P., Roskosz, M., & Ingrin, J. (2004). Redox state, microstructure and viscosity of a partially crystallized basalt melt. *Earth and Planetary Science Letters*, *218*(1–2), 31–44. https://doi.org/10.1016/S0012-821X(03)00641-1

Cassar, D. R. (2021). ViscNet: Neural network for predicting the fragility index and the temperature-dependency of viscosity. *Acta Materialia*, *206*, 116602. https://doi.org/10.1016/j.actamat.2020.116602

Cassidy, M., Manga, M., Cashman, K., & Bachmann, O. (2018). Controls on explosive-effusive volcanic eruption styles. *Nature Communications*, *9*(1), 2839. https://doi.org/10.1038/s41467-018-05293-3

Chevrel, M. O., Giordano, D., Potuzak, M., Courtial, P., & Dingwell, D. B. (2013). Physical properties of $CaAl_2Si_2O_8$–$CaMgSi_2O_6$–FeO–Fe_2O_3 melts: Analogues for extra-terrestrial basalt. *Chemical Geology*, *346*, 93–105. https://doi.org/10.1016/j.chemgeo.2012.09.004

Colucci, S., & Papale, P. (2021). Deep magma transport control on the size and evolution of explosive volcanic eruptions. *Frontiers of Earth Science*, *9*, 436. https://doi.org/10.3389/feart.2021.681083

Di Genova, D., Kolzenburg, S., Wiesmaier, S., Dallanave, E., Neuville, D. R., Hess, K.-U., & Dingwell, D. B. (2017). A compositional tipping point governing the mobilization and eruption style of rhyolitic magma. *Nature*, *552*(7684), 235–238. https://doi.org/10.1038/nature24488

Di Genova, D., Romano, C., Hess, K.-U., Vona, A., Poe, B. T., Giordano, D., et al. (2013). The rheology of peralkaline rhyolites from Pantelleria Island. *Journal of Volcanology and Geothermal Research*, *249*, 201–216. https://doi.org/10.1016/j.jvolgeores.2012.10.017

Dingwell, D. B. (1996). Volcanic dilemma–flow or blow? *Science*, *273*(5278), 1054–1055. https://doi.org/10.1126/science.273.5278.1054

Dingwell, D. B., Hess, K.-U., & Romano, C. (1998). Viscosity data for hydrous peraluminous granitic melts; comparison with a metaluminous model. *American Mineralogist*, *83*(3–4), 236–239. https://doi.org/10.2138/am-1998-3-406

Dingwell, D. B., Romano, C., & Hess, K.-U. (1996). The effect of water on the viscosity of a haplogranitic melt under PTX conditions relevant to silicic volcanism. *Contributions to Mineralogy and Petrology*, *124*(1), 19–28. https://doi.org/10.1007/s004100050170

Dingwell, D. B., & Virgo, D. (1987). The effect of oxidation state on the viscosity of melts in the system Na_2O-FeO-Fe_2O_3-SiO_2. *Geochimica et Cosmochimica Acta*, *51*(2), 195–205. https://doi.org/10.1016/0016-7037(87)90231-6

Duan, X. (2014). A model for calculating the viscosity of natural iron-bearing silicate melts over a wide range of temperatures, pressures, oxygen fugacities, and compositions. *American Mineralogist*, *99*(11–12), 2378–2388. https://doi.org/10.2138/am-2014-4841

Friedman, I., Long, W., & Smith, R. L. (1963). Viscosity and water content of rhyolite glass. *Journal of Geophysical Research*, *68*(24), 6523–6535. https://doi.org/10.1029/JZ068i024p06523

Fulcher, G. S. (1925). Analysis of recent measurements of the viscosity of glasses. *Journal of the American Ceramic Society*, *8*(6), 339–355. https://doi.org/10.1111/j.1151-2916.1925.tb16731.x

Giordano, D., Ardia, P., Romano, C., Dingwell, D. B., Di Muro, A., Schmidt, M. W., et al. (2009). The rheological evolution of alkaline Vesuvius magmas and comparison with alkaline series from the Phlegrean Fields, Etna, Stromboli and Teide. *Geochimica et Cosmochimica Acta*, *73*(21), 6613–6630. https://doi.org/10.1016/j.gca.2009.07.033

Giordano, D., & Dingwell, D. B. (2003a). Non-Arrhenian multicomponent melt viscosity: A model. *Earth and Planetary Science Letters*, *208*(3–4), 337–349. https://doi.org/10.1016/S0012-821X(03)00042-6

Giordano, D., & Dingwell, D. B. (2003b). Viscosity of hydrous Etna basalt: Implications for Plinian-style basaltic eruptions. *Bulletin of Volcanology*, *65*(1), 8–14. https://doi.org/10.1007/s00445-002-0233-2

Giordano, D., Dingwell, D. B., & Romano, C. (2000). Viscosity of a Teide phonolite in the welding interval. *Journal of Volcanology and Geothermal Research*, *103*(1–4), 239–245. https://doi.org/10.1016/S0377-0273(00)00226-2

Giordano, D., Mangiacapra, A., Potuzak, M., Russell, J. K., Romano, C., Dingwell, D. B., & Di Muro, A. (2006). An expanded non-Arrhenian model for silicate melt viscosity: A treatment for metaluminous, peraluminous and peralkaline liquids. *Chemical Geology*, *229*(1–3), 42–56. https://doi.org/10.1016/j.chemgeo.2006.01.007

Giordano, D., Romano, C., Papale, P., & Dingwell, D. B. (2004). The viscosity of trachytes, and comparison with basalts, phonolites, and rhyolites. *Chemical Geology*, *213*(1–3), 49–61. https://doi.org/10.1016/j.chemgeo.2004.08.032

Giordano, D., Russell, J. K., & Dingwell, D. B. (2008). Viscosity of magmatic liquids: A model. *Earth and Planetary Science Letters*, *271*(1–4), 123–134. https://doi.org/10.1016/j.epsl.2008.03.038

Gonnermann, H. M., & Manga, M. (2007). The fluid mechanics inside a volcano. *Annual Review of Fluid Mechanics*, *39*(1), 321–356. https://doi.org/10.1146/annurev.fluid.39.050905.110207

Gonnermann, H. M., & Manga, M. (2013). Chapter 4: Dynamics of magma ascent in the volcanic conduit. In S. A. Fagents, T. K. P. Gregg, & R. M. C. E. Lopes (Eds.), *Modeling volcanic processes: The physics and mathematics of volcanism* (pp. 55–84). Cambridge University Press. https://doi.org/10.1017/CBO9781139021562.004

Goto, A., Taniguchi, H., & Kitakaze, A. (2005). Viscosity measurements of hydrous rhyolitic melts using the fiber elongation method. *Bulletin of Volcanology*, *67*(6), 590–596. https://doi.org/10.1007/s00445-004-0401-7

Harris, C. R., Millman, K. J., van der Walt, S. J., Gommers, R., Virtanen, P., Cournapeau, D., et al. (2020). Array programming with NumPy. *Nature*, *585*(7825), 357–362. https://doi.org/10.1038/s41586-020-2649-2

Hellwig, B. M. (2006). *The viscosity of dacitic liquids measured at conditions relevant to explosive arc volcanism: Determing the influence of temperature, silicate composition, and dissolved volatile content* (Unpublished doctoral dissertation). University of Missouri–Columbia.

Hess, K.-U., Dingwell, D. B., & Webb, S. L. (1995). The influence of excess alkalis on the viscosity of a haplogranitic melt. *American Mineralogist*, *80*(3–4), 297–304. https://doi.org/10.2138/am-1995-3-412

Hofmeister, A. M., Sehlke, A., Avard, G., Bollasina, A. J., Robert, G., & Whittington, A. G. (2016). Transport properties of glassy and molten lavas as a function of temperature and composition. *Journal of Volcanology and Geothermal Research*, *327*, 330–348. https://doi.org/10.1016/j.jvolgeores.2016.08.015

Hofmeister, A. M., Whittington, A. G., Goldsand, J., & Criss, R. G. (2014). Effects of chemical composition and temperature on transport properties of silica-rich glasses and melts. *American Mineralogist*, *99*(4), 564–577. https://doi.org/10.2138/am.2014.4683

Hui, H., & Zhang, Y. (2007). Toward a general viscosity equation for natural anhydrous and hydrous silicate melts. *Geochimica et Cosmochimica Acta*, *71*(2), 403–416. https://doi.org/10.1016/j.gca.2006.09.003

Kingma, D. P., & Ba, J. (2014). Adam: A method for stochastic optimization. *arXiv preprint arXiv:1412.6980*. https://doi.org/10.48550/arXiv.1412.6980

Kolzenburg, S., Di Genova, D., Giordano, D., Hess, K.-U., & Dingwell, D. B. (2018). The effect of oxygen fugacity on the rheological evolution of crystallizing basaltic melts. *Earth and Planetary Science Letters*, *487*, 21–32. https://doi.org/10.1016/j.epsl.2018.01.023

Langhammer, D., Di Genova, D., & Steinle-Neumann, G. (2021). Modeling the viscosity of anhydrous and hydrous volcanic melts. *Geochemistry, Geophysics, Geosystems*, *22*(8), e2021GC009918. https://doi.org/10.1029/2021GC009918

Le Bas, M. J., Le Maitre, R. W., Streckeisen, A., & Zanettin, B. (1986). A chemical classification of volcanic rocks based on the total alkali-silica diagram. *Journal of Petrology*, *27*(3), 745–750. https://doi.org/10.1093/petrology/27.3.745

Le Losq, C., & Neuville, D. R. (2013). Effect of the Na/K mixing on the structure and the rheology of tectosilicate silica-rich melts. *Chemical Geology*, *346*, 57–71. https://doi.org/10.1016/j.chemgeo.2012.09.009

Le Losq, C., Valentine, A. P., Mysen, B. O., & Neuville, D. R. (2021). Structure and properties of alkali aluminosilicate glasses and melts: Insights from deep learning. *Geochimica et Cosmochimica Acta*, *314*, 27–54. https://doi.org/10.1016/j.gca.2021.08.023

Liebske, C., Behrens, H., Holtz, F., & Lange, R. A. (2003). The influence of pressure and composition on the viscosity of andesitic melts. *Geochimica et Cosmochimica Acta*, *67*(3), 473–485. https://doi.org/10.1016/S0016-7037(02)01139-0

Mauro, J. C., Yue, Y., Ellison, A. J., Gupta, K., & Allan, D. C. (2009). Viscosity of glass-forming liquids. *Proceedings of the National Academy of Sciences of the United States of America*, *106*(47), 19780–19784. https://doi.org/10.1073/Proc.Natl.Acad.Sci.U.S.A.0911705106

Misiti, V., Freda, C., Taddeucci, J., Romano, C., Scarlato, P., Longo, A., et al. (2006). The effect of H_2O on the viscosity of K-trachytic melts at magmatic temperatures. *Chemical Geology*, *235*(1–2), 124–137. https://doi.org/10.1016/j.chemgeo.2006.06.007

Misiti, V., Vetere, F., Freda, C., Scarlato, P., Behrens, H., Mangiacapra, A., & Dingwell, D. B. (2011). A general viscosity model of Campi Flegrei (Italy) melts. *Chemical Geology*, *290*(1–2), 50–59. https://doi.org/10.1016/j.chemgeo.2011.08.010

Misiti, V., Vetere, F., Mangiacapra, A., Behrens, H., Cavallo, A., Scarlato, P., & Dingwell, D. B. (2009). Viscosity of high-K basalt from the 5th April 2003 Stromboli paroxysmal explosion. *Chemical Geology*, *260*(3–4), 278–285. https://doi.org/10.1016/j.chemgeo.2008.12.023

Montavon, G., Orr, G., & Müller, K.-R. (2012). *Neural networks: Tricks of the trade* (Vol. 7700). Springer.

Morrison, A. A., Whittington, A. G., Smets, B., Kervyn, M., & Sehlke, A. (2020). The rheology of crystallizing basaltic lavas from Nyiragongo and Nyamuragira volcanoes, DRC. *Volcanica*, *3*, 1–28. https://doi.org/10.30909/vol.03.01.0128

Morrison, A. A., Zanetti, M., Hamilton, C. W., Lev, E., Neish, C. D., & Whittington, A. G. (2019). Rheological investigation of lunar highland and mare impact melt simulants. *Icarus*, *317*, 307–323. https://doi.org/10.1016/j.icarus.2018.08.001

Neuville, D. R., Courtial, P., Dingwell, D. B., & Richet, P. (1993). Thermodynamic and rheological properties of rhyolite and andesite melts. *Contributions to Mineralogy and Petrology*, *113*(4), 572–581. https://doi.org/10.1007/BF00698324

O'Malley, T., Bursztein, E., Long, J., Chollet, F., Jin, H., Invernizzi, L., et al. (2019). Kerastuner. Retrieved from https://github.com/keras-team/keras-tuner

Papale, P. (1999). Strain-induced magma fragmentation in explosive eruptions. *Nature*, *397*(6718), 425–428. https://doi.org/10.1038/17109

Reback, J., McKinney, W., Van Den Bossche, J., Augspurger, T., Cloud, P., Klein, A., et al. (2021). *pandas-dev/pandas: Pandas 1.3.4*. Zenodo. https://doi.org/10.5281/zenodo.3509134

Reddi, S. J., Kale, S., & Kumar, S. (2019). On the convergence of Adam and beyond. *arXiv preprint arXiv:1904.09237*. https://doi.org/10.48550/arXiv.1904.09237

Richet, P., Lejeune, A.-M., Holtz, F., & Roux, J. (1996). Water and the viscosity of andesite melts. *Chemical Geology*, *128*(1–4), 185–197. https://doi.org/10.1016/0009-2541(95)00172-7

Robert, G. (2014). *The effects of volatiles on the viscosity and heat capacity of calc-alkaline basaltic and basaltic andesite liquids* (Doctoral Dissertation). University of Missouri.

Robert, G., Knipping, J. L., Scherbarth, S., Robertson, T. E., Stechern, A., Behrens, H., & Whittington, A. G. (2015). Heat capacity and viscosity of basaltic melts with $H_2O \pm F \pm CO_2$. *Chemical Geology*, *418*, 51–65. https://doi.org/10.1016/j.chemgeo.2014.07.015

Robert, G., Smith, R. A., & Whittington, A. G. (2019). Viscosity of melts in the $NaAlSiO_4$-$KAlSiO_4$-SiO_2 system: Configurational entropy modelling. *Journal of Non-Crystalline Solids*, *524*, 119635. https://doi.org/10.1016/j.jnoncrysol.2019.119635

Robert, G., Whittington, A., Stechern, A., & Behrens, H. (2013). The effect of water on the viscosity of a synthetic calc-alkaline basaltic andesite. *Chemical Geology*, *346*, 135–148. https://doi.org/10.1016/j.chemgeo.2012.10.004

Romano, C., Giordano, D., Papale, P., Mincione, V., Dingwell, D. B., & Rosi, M. (2003). The dry and hydrous viscosities of alkaline melts from Vesuvius and Phlegrean Fields. *Chemical Geology*, *202*(1–2), 23–38. https://doi.org/10.1016/S0009-2541(03)00208-0

Romine, W. L., & Whittington, A. G. (2015). A simple model for the viscosity of rhyolites as a function of temperature, pressure and water content. *Geochimica et Cosmochimica Acta*, *170*, 281–300. https://doi.org/10.1016/j.gca.2015.08.009

Sehlke, A., & Whittington, A. G. (2015). Rheology of lava flows on Mercury: An analog experimental study. *Journal of Geophysical Research: Planets*, *120*(11), 1924–1955. https://doi.org/10.1002/2015JE004792

Sehlke, A., & Whittington, A. G. (2016). The viscosity of planetary tholeiitic melts: A configurational entropy model. *Geochimica et Cosmochimica Acta*, *191*, 277–299. https://doi.org/10.1016/j.gca.2016.07.027

Snoek, J., Larochelle, H., & Adams, R. P. (2012). Practical Bayesian optimization of machine learning algorithms. *Advances in Neural Information Processing Systems*, *25*.

Srivastava, N., Hinton, G., Krizhevsky, A., Sutskever, I., & Salakhutdinov, R. (2014). Dropout: A simple way to prevent neural networks from overfitting. *Journal of Machine Learning Research*, *15*, 1929–1958.

Stabile, P., Sicola, S., Giuli, G., Paris, E., Carroll, M. R., Deubener, J., & Di Genova, D. (2021). The effect of iron and alkali on the nanocrystal-free viscosity of volcanic melts: A combined Raman spectroscopy and DSC study. *Chemical Geology*, *559*, 119991. https://doi.org/10.1016/j.chemgeo.2020.119991

Stabile, P., Webb, S., Knipping, J. L., Behrens, H., Paris, E., & Giuli, G. (2016). Viscosity of pantelleritic and alkali-silicate melts: Effect of Fe redox state and Na/(Na + K) ratio. *Chemical Geology*, *442*, 73–82. https://doi.org/10.1016/j.chemgeo.2016.09.003

Tammann, G., & Hesse, W. (1926). Die Abhängigkeit der Viskosität von der Temperatur bei unterkühlten Flüssigkeiten. *Zeitschrift für anorganische und allgemeine Chemie*, *156*(1), 245–257. https://doi.org/10.1002/zaac.19261560121

Tandia, A., Onbasli, M. C., & Mauro, J. C. (2019). Machine learning for glass modeling. In *Springer handbook of glass* (pp. 1157–1192). Springer.

Vetere, F., Behrens, H., Holtz, F., & Neuville, D. R. (2006). Viscosity of andesitic melts—New experimental data and a revised calculation model. *Chemical Geology*, *228*(4), 233–245. https://doi.org/10.1016/j.chemgeo.2005.10.009

Vetere, F., Behrens, H., Misiti, V., Ventura, G., Holtz, F., De Rosa, R., & Deubener, J. (2007). The viscosity of shoshonitic melts (Vulcanello Peninsula, Aeolian Islands, Italy): Insight on the magma ascent in dikes. *Chemical Geology*, *245*(1–2), 89–102. https://doi.org/10.1016/j.chemgeo.2007.08.002

Vetere, F., Behrens, H., Schuessler, J. A., Holtz, F., Misiti, V., & Borchers, L. (2008). Viscosity of andesite melts and its implication for magma mixing prior to Unzen 1991–1995 eruption. *Journal of Volcanology and Geothermal Research*, *175*(1–2), 208–217. https://doi.org/10.1016/j.jvolgeores.2008.03.028

Vogel, H. (1921). Das Temperaturabhängigkeitsgesetz der Viskosität von Flüssigkeiten. *Physikalische Zeitschrift*, *22*, 645–646.

Webb, S. L. (2021). Viscosity of evolving magmas: A case study of the glass House Mountains, Australia. *Bulletin of Volcanology*, *83*(11), 1–12. https://doi.org/10.1007/s00445-021-01495-8

Whittington, A. G., Bouhifd, M. A., & Richet, P. (2009). The viscosity of hydrous $NaAlSi_3O_8$ and granitic melts: Configurational entropy models. *American Mineralogist*, *94*, 1–16. https://doi.org/10.2138/am.2009.2892

Whittington, A. G., Hellwig, B. M., Behrens, H., Joachim, B., Stechern, A., & Vetere, F. (2009). The viscosity of hydrous dacitic liquids: Implications for the rheology of evolving silicic magmas. *Bulletin of Volcanology*, *71*(2), 185–199. https://doi.org/10.1007/s00445-008-0217-y

Whittington, A. G., Richet, P., Behrens, H., Holtz, F., & Scaillet, B. (2004). Experimental temperature–X(H_2O)–viscosity relationship for leucogranites and comparison with synthetic silicic liquids. *Earth and Environmental Science Transactions of The Royal Society of Edinburgh*, *95*(1–2), 59–71. https://doi.org/10.1017/S0263593300000924

Whittington, A. G., Richet, P., & Holtz, F. (2000). Water and the viscosity of depolymerized aluminosilicate melts. *Geochimica et Cosmochimica Acta*, *64*(21), 3725–3736. https://doi.org/10.1016/S0016-7037(00)00448-8

Whittington, A. G., Richet, P., Linard, Y., & Holtz, F. (2001). The viscosity of hydrous phonolites and trachytes. *Chemical Geology*, *174*(1–3), 209–223. https://doi.org/10.1016/S0009-2541(00)00317-X

Zheng, Q., Mauro, J. C., Ellison, A. J., Potuzak, M., & Yue, Y. (2011). Universality of the high-temperature viscosity limit of silicate liquids. *Physical Review B: Condensed Matter*, *83*(21), 212202. https://doi.org/10.1103/PhysRevB.83.212202